Cation and Water Structure, Dynamics and Energetics in Smectite Clays: A Molecular Dynamics Study of Ca-Hectorite

Narasimhan Loganathan[1], A. Ozgur Yazaydin[1,2], Geoffrey M. Bowers[3], Andrey G. Kalinichev[4] and R. James Kirkpatrick[5]

[1] Department of Chemistry, Michigan State University, East Lansing, Michigan 48824, United States

[2] Department of Chemical Engineering, University College London, London, WC1E 7JE, United Kingdom

[3] Division of Chemistry, Alfred University, Alfred, New York 14802, United States

[4] Laboratoire SUBATECH (UMR-6457), Ecole des Mines de Nantes, 44307, Nantes, France

[5] College of Natural Science, Michigan State University, East Lansing, Michigan 48824, United States

[*)] **Corresponding author e-mail:** naresh20@msu.edu

Tel: (+1)517-353-1106

ABSTRACT

The incorporation of Ca^{2+} into smectite minerals is well known to have a significant effect on the swelling behavior and mechanical properties of this environmentally and technologically important group of materials. Relative to common alkali cations such as Na^{+}, K^{+}, and Cs^{+}, Ca^{2+} has a larger charge/ionic radius ratio, and thus interacts very differently with interlayer water molecules and the oxygens of the clay basal surface. Recent ^{2}H and ^{43}Ca NMR studies of the smectite mineral, hectorite, show that the molecular scale interlayer dynamics is quite different with Ca^{2+} than with alkali cations. Classical molecular dynamics (MD) simulations presented here use a newly developed hectorite model with a disordered distribution of Li^{+}/Mg^{2+} substitutions in the octahedral sheet and provide new insight into the origin of the effects of Ca^{2+} on the structure, dynamics and energetics of smectite interlayers. The computed basal spacings and thermodynamic properties suggest the potential for formation of stable mono-layer hydrates that have partial and complete water contents, a bilayer hydrate, and possible expansion to higher hydration states. The system hydration energies are comparable to those previously calculated for Ca-montmorillonite[21,53] and are more negative than for Cs- and Na-hectorite, due to the higher hydration energy of Ca^{2+}. The coordination environments of Ca^{2+} change significantly with increasing interlayer hydration, with the extent of coordination to basal oxygens decreasing as the number of interlayer molecules increases. On external (001) surfaces, the H_2O molecules closest to the surface are adsorbed at the centers of ditrigonal cavities and bridge Ca^{2+} to the surface. The Ca^{2+} ions on the external surface are all in outer sphere coordination with the basal oxygens of the surface, and the proximity-restricted region with a significant number of Ca^{2+} is approximately 6 Å thick. Quantification of these interactions provides a basis for understanding intercalation of Ca^{2+} by organic species and smectite minerals.

INTRODUCTION

Clay minerals are abundantly present in nature and are important components of many soils, sediments and sedimentary rocks. The low hydraulic conductivities and high retention capacities of clay materials for many organic and inorganic contaminants make them important in numerous geochemical and environmental situations.[1-5] For instance, clay formations are often considered as potential hosts for geological disposal of long-lived radioactive waste.[6-9] They are also essential in pharmaceutical and cosmetic products, in mining operations, and as catalysts.[10-13] Smectite clays can be particularly important geochemically and as components of engineered barriers because of their swelling capacity and ability to limit transport of toxic waste away from repository sites through sorption into interlayer galleries.[6-9,14,15] These properties occur in large part because the structural and dynamical properties of ions and water molecules in the hydrated smectite interlayers are greatly modified compared to bulk aqueous ionic solutions. Interlayer expansion of smectites strongly depends on temperature, external pressure, the smectite composition and the location of its negative structural charge.[16-21]

In recent years, the structure and dynamics of metal ions and H_2O molecules in hectorite have been extensively studied experimentally using quasi-elastic neutron scattering (QENS), nuclear magnetic resonance (NMR) and X-ray diffraction (XRD) techniques.[22-35] The results clearly indicate that H_2O diffusion is 4 to 5 times slower in the interlayer than in bulk solution and that the structure, dynamics and energetics of interlayer water are strongly controlled by the nature of the interlayer cations and their hydration energies. It is, however, difficult to provide a detailed, molecular scale interpretation of the experimental data or to experimentally distinguish between the behavior of ions and H_2O molecules located in the interlayer galleries and on external particle surfaces (inter-particle pores). As a consequence, atomistic computer simulations using molecular

dynamics (MD) and Monte Carlo (MC) methods have become important tools to investigate the structure, dynamics, and energetics of hydrated species in and on smectites and other layer structure materials, complementing experimental measurements.[1,16-20, 36-45] For instance, the results show that the close association of the cations, water molecules and basal oxygen atoms in the smectite interlayers can significantly decrease the rates of their diffusion compared to when these species are found in inter-particle pores.[46, 47]

The incorporation of Ca^{2+} into smectite minerals is well known to have a significant effect on the swelling behavior and mechanical properties relative to common alkali cations such as Na^{+}, K^{+}, and Cs^{+}. Ca^{2+} has a larger charge/ionic radius ratio and hydration energy than these alkali cations[21] and thus interacts very differently with interlayer water molecules and the oxygens of the clay basal surface. Most experimental and computational studies of Ca^{2+} in smectites have focused on montmorillonite and beidellite.[16,17,21,36-39,48-53] There have been fewer studies of hectorite, despite its wide technological application and its structural similarity to montmorillonite. Because of its large hydration energy and, thus, high affinity for H_2O molecules, the dominant interactions of Ca^{2+} in smectite interlayers and on external surfaces is with H_2O molecules rather than with the basal oxygens (O_b) of the smectite layers. These interactions also significantly affect the behavior of organic matter with respect to hectorite and other smectites,[40, 54, 55] which in turn can greatly alter the mobility of aqueous species in soils and sediments. The presence of Ca^{2+} is well known to affect the aggregation of organic matter.[56, 57] Thus, molecular scale understanding of these interactions can have practical implications in determining the performance of geochemical transport models.

Morrow et al.[41] have recently reviewed the extensive literature on computational modeling of smectite minerals and also report the effect of varying hydration state on the thermodynamic

stability, interlayer structure, and diffusion of Na^+ ions in hectorite interlayers. The results show that Na^+ is preferentially adsorbed as outer sphere complexes with increasing hydration level and that the H_2O molecules diffuse an order of magnitude slower in the interlayers when compared to bulk, even in two water layer hydrates. Similar studies of the external surfaces of montmorillonite and hectorite by Greathouse et al.[42] show that Na^+ and H_2O diffusion in the proximity-restricted region (approximately within 10 Å from the clay surface in their results) is faster compared to interlayers but still lower than in bulk solution. Recent simulations by Teich-McGoldrick et al.[21] indicate that Ca-montmorillonite occurs as a bilayer hydrate under ambient conditions. The results also suggest an increase in interlayer spacing at higher temperatures because of the increased thermal motion of the interlayer species. Concurrently, MD simulations of the interlayers and external surfaces of hectorite and other smectites exchanged with Cs^+, which has a much lower hydration energy than Ca^{2+}, show that Cs^+ is preferentially coordinated to the O_b atoms, that the interlayer structure, dynamics, and expansion energetics is much different than with Ca^{2+}, and that the Cs^+ structural environments and dynamics are strongly correlated with reorientation of the structural OH^- groups of the substrate clay.[43, 44]

Hectorite is widely used in NMR studies,[22-27, 55,58] because samples with low Fe contents are readily available. The low Fe content allows for higher resolution spectra than for most other natural smectites, because it minimizes paramagnetic effects on the probe nuclei. Bowers et al. [24] used NMR and XRD measurements to show that Ca^{2+} ions are adsorbed on hectorite at several relative humidities (RHs) as outer sphere complexes with tightly held H_2O molecules in their first coordination shell. However, these studies could not resolve interlayer from surface species, which is likely to be important in understanding the interaction of organic molecules with smectites.[40, 54]

This paper presents the results of MD simulation study of Ca-exchanged hectorite that provides otherwise unobtainable molecular scale insight into understanding of the experimental results. The specific objectives are (1) to characterize the structure and energetics of Ca^{2+} adsorption as functions of H_2O content; (2) to understand the relationships between the coordination environments of surface and interlayer H_2O molecules and the H_2O and Ca^{2+} dynamics; and (3) to illustrate the effects of cation hydration energy by comparing the results to those for Cs- and Na-hectorite. The results are in good agreement with available experimental NMR and XRD data.[24,25,27-29] Because both hectorite and montmorillonite develop their structural charge in the octahedral sheet of the T-O-T clay layers, we also compare our results to previously published simulations for montmorillonite.[21, 53]

SIMULATION DETAILS

Hectorite is a 2:1 trioctahedral smectite clay with an octahedral layer sandwiched between two layers of SiO_4 tetrahedra. It develops a net negative structural charge due to isomorphic Li^+ for Mg^{2+} substitution in the octahedral layer that is compensated by interlayer cations. The structural formula of our hectorite simulation model is $M^+(Mg_5Li)Si_8O_{20}(OH)_4$, and the structure is based on that of Breu et al.[59] The simulated Li^+/Mg^{2+} ratio of 1/5 is similar to that of the natural San Bernardino hectorite used in our experimental XRD and NMR studies.[24-26] There is no tetrahedral Al^{3+}/Si^{4+} substitution in our simulated models, in good agreement with the experimental sample, which has only a very small fraction (0.25%) of tetrahedral substitution. However, the natural hectorite contains both OH^- and F^- coordinated to the octahedral cations, whereas the simulation model contains only OH^-. The hydration of synthetic fluoro-hectorite has been discussed previously.[1,32-36,60]

The simulation supercell used to investigate the interlayer galleries consists of 40 crystallographic unit cells of hectorite (5 × 4 × 2) and encompasses two interlayers. The lateral dimensions of the simulated model are approximately 26 Å × 36 Å and are large enough to avoid any finite size effects. This size also allows for a disordered distribution of Li^+/Mg^{2+} isomorphic substitutions in the octahedral layer and thus of the associated structural charge (Figure 1). The Li^+/Mg^{2+} distribution was imposed only after the unit cell was replicated in all crystallographic directions to the full size of the simulation supercell. This procedure provides a simulation supercell in which each TOT layer has a different arrangement of Li^+ ions in the octahedral sheet. The distribution is not entirely random, however, because no Li-O-Li linkages were allowed (a condition analogous to Lowenstein's aluminum avoidance rule[61]), and there is, thus, no concentration of structural charge around individual substituted octahedral sites. All the Na^+ ions in the initial model were replaced by Ca^{2+} ions (one Ca^{2+} for every two Na^+), which were initially placed at the mid-plane of the interlayers. A broad range of water contents from 0 to 420 mg_{H2O}/g_{clay} (0 to ~35 H_2O/formula unit) was used to study the effect of hydration on the interlayer expansion and associated energetics. The basal spacing of the model at each hydration level was initially set slightly larger than the expected final value and was allowed to relax during the equilibration stage of the MD run. Since the clay layer charge in our system is -1.0|*e*| per crystallographic unit cell, the quantitative measure of water content expressed as H_2O/Ca^{2+} or H_2O/(unit cell) in our case is numerically the same.

The simulation cell for modeling the external surface was built by cleaving the hectorite structure along the (001) plane at the middle of the interlayer space, with each basal surface retaining one-half of the Ca^{2+} ions. The simulation cell consisted of 3 hectorite layers with a total thickness of ~25 Å. The lateral dimensions were ~72 Å, and the total distance between the cleaved

surfaces ~120 Å. The large nanopore thickness perpendicular to the surface effectively eliminates the influence of one surface on the other when the periodic boundary conditions are applied. Initially, H_2O slabs with a thickness of ~50 Å were placed on each of the two cleaved hectorite (001) surfaces, resulting in a ~15 Å vapor phase formed at the middle of the nanopore. Previous simulation studies have indicated that water films this thick are sufficient to prevent significant interaction between the two surfaces, thus creating two statistically independent interfaces.[18, 40, 62-65] All Ca^{2+} ions were initially placed in the aqueous slabs ~15 Å away from the hectorite surface, which allowed them to freely assume their interfacial structural environments during the course of the simulation. The isomorphic Li^{+}/Mg^{2+} distribution in the octahedral sheet was obtained in the same way as for the interlayer models.

MD simulations using the isobaric-isothermal *NPT* ensemble (constant number of atoms *N*, constant pressure *P,* and constant temperature *T*) and the canonical *NVT* ensemble (constant volume *V*) were performed with the LAMMPS simulations package.[66] A Nosé-Hoover thermostat and barostat were used to control the temperature and the pressure separately in all 3 dimensions.[67, 68] A time step of 1 fs was used, and three dimensional periodic boundary conditions were employed with a cutoff of 10.0 Å for short range non-electrostatic interactions. Ewald summation was used for computing long-range electrostatic interactions with an accuracy of 10^{-4}. The interatomic interactions for all species in the system were obtained using the *CLAYFF* force field[69], which is used widely in environmental and materials science simulations.[70,71] The flexible SPC water model is incorporated into *CLAYFF* and is used here.[72] For each modeled system, *NPT* simulations were first carried out at ambient conditions (*P*=1 bar and *T*=300 K) for 4 ns to reach equilibration. This was followed by a 4 ns *NPT* data production run, during which the data were recorded every 10 fs. All the thermodynamic properties were calculated using the data from the last 3 ns of the

equilibrium MD trajectory. The thermodynamic properties and cell dimensions for each hydration state were calculated using statistical averages over 10 equal time blocks (300 ps each). This method yields high confidence levels for the reported mean values. Potentially stable hydration states were determined from thermodynamic analysis of the *NPT* simulations of the systems with hydrated interlayers. Structural and dynamic properties were then obtained from subsequent *NVT* simulations, which were performed for another 2 ns of equilibration and 2 ns of data production. The initial atomic positions for the *NVT* simulations were the mean values of *NPT* configurations during the last 3 ns. *NVT* simulations of the external basal surface were performed in a manner similar to interlayer simulations under ambient conditions for 3 ns of equilibration and additional 4 ns of data production with data collection every 10 fs. The data from the last 2 ns of the *NVT* simulation runs were used to determine the structural and dynamical properties.

The swelling properties of hydrated Ca-hectorite were quantitatively analyzed in terms of the basal spacings, the hydration and immersion energies, and the isosteric heats of adsorption. The methodologies used to obtain the thermodynamic properties have been discussed in detail in previous studies[16,21,43,47] and hence provided in the supporting information. Structural properties of the clay interlayers at different states of hydration were analyzed using probability density distributions both parallel and perpendicular to the hectorite surface. The time averaged position of the basal surface formed by the bridging oxygen atoms, O_b, was taken as a reference ($z = 0$) for all interfacial atomic density profiles. The H-bonding networks in the interlayer galleries and on the external basal surface were analyzed by applying commonly used geometric criteria by which an H-bond is assumed to exist if: (i) their intermolecular O···H distance is less than 2.45 Å, and (ii) the angle between the intermolecular O···O vector and the direction of the covalent H-O bond of the donor is less than 30º.[73-75] For the present analysis of the interfacial H-bonding network the

oxygen atoms of clay surface, O_b, were treated as potential H-bond acceptors in the same way as the oxygen atoms of the H_2O molecules (O_{H2O}). Diffusion coefficients of the interlayer H_2O molecules were calculated in a standard way using mean-square displacements, with full understanding that the mobility of the interlayer species is quasi-two-dimensional.

The dynamical properties of H_2O molecules and Ca^{2+} ions were quantitatively characterized by calculation of residence times for nearest neighbor coordination of the O_b atoms, Ca^{2+} ions and H_2O molecules. These residence times were evaluated using two different time correlation functions. The intermittent residence time, $c(t)$, is given a value of 1 only when two species are coordinated (present in the first coordination sphere of each other), and is otherwise 0. For this definition, the pair is considered coordinated, even if their coordination is temporarily broken and then re-established during the analysis time. The continuous residence time, $C(t)$ is defined similarly, except the species are not considered coordinated if their coordination is lost even for a short period during the analysis time.[73-76] The functions $c(t)$ and $C(t)$ were calculated at time intervals of 2 ps, because this time reflects the exchange rate of H_2O molecules in the hydration shells of metal ions.[77] It also represents a typical hydrogen bond lifetime in liquid H_2O under ambient conditions.[73-76] The procedure described by Luzar et al.[73,74] is followed to compute the residence times for all pairs. A detailed discussion of these residence times and how they are calculated is provided in references 73-76, and our application of this analytical tools is similar to those in numerous other simulation studies.[16-21,39-41,43,53,62,64,65,76]

RESULTS AND DISCUSSION

Ca-Hectorite Swelling and Hydration Energetics

The computed variation of interlayer spacing as a function of water content suggests the potential for formation of distinct and well defined mono-layer hydrates with partially and fully filled interlayers, a bi-layer hydrate, and continuous expansion with increasing water content beyond the bi-layer hydrate (Figure 2a). The computed interlayer spacing of a completely dehydrated Ca-hectorite (no interlayer H_2O) is 9.6 Å, in good agreement with recent simulations of Ca-montmorillonite that give values of ~9.4 Å.[21, 53] Since the ionic radii of Ca^{2+} and Na^{+} ions are similar (~1.1Å), the basal spacings of dry Na- and Ca-hectorite are also quite similar (Table 1).[21,41,53] In contrast, the interlayer spacing of dry Cs-hectorite is noticeably larger (10.65 Å). [20,43,44] The mono- and bi-layer hydrates of Ca-hectorite are characterized by distinct plateaus in the basal spacing at ~12.3 Å and 14.9 Å, respectively. The basal spacings of the partially and fully filled mono-layer structures are quite similar (12.25 and 12.34 Å, respectively), showing that the filling of vacant spaces between Ca^{2+} by water molecules has little effect on the macroscopic basal spacing. The calculated values are in good agreement with basal spacings experimentally measured for Ca-hectorite by powder X-ay diffraction (Table 1).[24,27-29] They are also in good agreement with previously published simulated values for Ca-montmorillonite and Na-hectorite, although the H_2O/cation ratios for the different structures are different.[21,41,53] For instance, the H_2O/Ca^{2+} ratios of Ca-hectorite corresponding to the fully filled mono-layer and the bi-layer hydrates are 9.0 and 16.0, whereas they are 6.0 and 20.0 for Ca-montmorillonite.[21,53] For Na-hectorite, the H_2O/Na^{+} ratios of the mono- and bi-layer hydrates are 3.0 and 10.0, respectively. These values correlate with the smaller charge density of Na^{+}, and its lower affinity for H_2O molecules,[41] but are primarily explained by the fact that there are twice as many monovalent Na^{+} ions as divalent Ca^{2+} ions present in the interlayer to compensate the same amount of clay structural charge. The H_2O/Cs^{+} ratios of the mono- and bi-layer hydrates of Cs-hectorite are similar to those of Na-hectorite,

despite the larger ionic radius and lower charge density of Cs^+.[41,43] Together, these observations clearly confirm that the affinity of the cations for H_2O molecules plays an important role in determining the interlayer spacing in humid environments.[20,43,44]

One important difference between the computed and experimental basal spacings of Ca-hectorite is that the experimentally observed basal spacings of samples held over P_2O_5, i.e., nominally dehydrated at ~0% relative humidity, are significantly larger, 12.8 Å[24,27] and 12.9 Å,[28,29] than the computed values. This 3.2-3.3 Å difference is much larger than experimental or computational error and is approximately equal to the diameter of a water molecule, suggesting that the experimental Ca-hectorite samples may always contain at least a partially filled H_2O molecular layer, even at 0% RH at room temperature. This contrasts with the behavior of Na-hectorite, which collapses to 0 water layers by drying under P_2O_5 at room temperature, and reflects the greater affinity of Ca^{2+} for H_2O molecules.[22]

The computed interlayer hydration energies for Ca-hectorite (Figure 2b) show minima at H_2O/Ca^{2+} ratios of 3-6.5, 9.0 and 12-16 associated with energies of -67, -61 and -58 kJ/mol respectively. The minima at 9.0 and 16.0 correspond to the filled mono-layer and bi-layer hydrates, and the minimum at ~6.5 is the partially filled mono-layer hydrate. The hydration energies of Ca-hectorite at all the simulated hydration levels are significantly lower than the bulk internal energy of SPC water (-41.4 kJ/mol), as also observed in previous MD simulation studies of Ca-montmorillonite.[21,41,53] This large difference indicates the potential for expansion to larger basal spacings. The values of the minima are also within a few kJ/mol of each other. Together, these results suggest that all the energetically well-defined hydration states of Ca-smectites and also hydration states beyond the bi-layer hydrate are potentially accessible at different externally imposed water activities (RHs). The sharp increase in hydration energy at water contents less than

~3.5 H_2O/Ca^{2+} clearly indicates that such states with nearly full removal of interlayer H_2O are energetically unfavorable, in good agreement with the experimental observation of basal spacings representative of a mono-layer hydrate at very low RHs and room temperature.[24, 27-29] The variation in hydration energy with hydration level is generally similar for Ca-hectorite and Ca-montmorillonite, which has energy minima of approximately -70 kJ/mol and -60 kJ/mol for the mono-layer and bi-layer hydrates respectively.[21, 53] The computed interlayer hydration energies of Na- and Cs-hectorite are always less negative than that of Ca-hectorite due to the greater affinity of Ca^{2+} for H_2O molecules.[20, 21, 41, 43, 44, 53]

The computed immersion energies of Ca-hectorite (Figure 2c) show shallow minima at ~6.5, 9.0 and 16.0 H_2O/Ca^{2+}, consistent with the computed hydration energies. These energy minima are not well localized. The continuous adsorption of H_2O molecules with decrease in energy after the formation of a monolayer hydrate indicates that the bi-layer hydrate is the one of the stable states for Ca-hectorites under ambient conditions. Further adsorption of H_2O molecules beyond the bi-layer hydrate is characterized by little variation in the immersion energies, indicating only a small energy cost to add or remove a water molecule, consistent with the idea that higher hydration states are possible. This result is in excellent agreement with experimental observations that show a monolayer hydrate at low relative humidity (RH) conditions, a bi-layer hydrate at moderate RH (43%),[24,27] and an ~4 layer hydrate for paste samples with a H_2O/clay ratio of 1.5 by weight.[25] Recently reported immersion energies for Ca-montmorillonite demonstrate a comparable trend, with the energies of the bi-layer, tri-layer and 4-layer hydrates being all very similar.[53] In contrast, the immersion energies of Cs-hectorite show well-defined energy barriers between the stable monolayer and hypothetical bi- and tri-layer hydration states.[43] We describe below the

structural and dynamic properties of the partial and complete mono-layer hydrates and the bi-layer hydrate.

Atomic Density Profiles

The atomic density profiles (ADPs) of Ca^{2+} ions and H_2O molecules as functions of distance normal to the basal hectorite surface for the hydrated interlayer galleries and external surfaces (Figures 3a-3d), provide detailed structural information essential to interpret the thermodynamic results. The ADP of the partial mono-layer hydrate with a H_2O/Ca^{2+} ratio of 6.5 consists of a single peak for Ca^{2+}, three peaks for O_{H2O}, and four peaks for H_{H2O} (Figure 3a). The Ca^{2+} ions are located at the center of the interlayer ~2.75 Å from both basal surfaces. These distances show that the Ca^{2+} ions occur in inner sphere (IS) coordination by O_b of the both sides of the interlayer, which are located at 0 Å and 5.5 Å (dark blue lines in Figure 3). The O_{H2O} peaks located at 1.7 Å and 3.8 Å represent the same types of adsorption sites related to the left and right interlayer surfaces. The slightly split O_{H2O} peak near the center of the interlayer represents H_2O molecules located near the plane occupied by the Ca^{2+} ions. The four peaks for H_{H2O} are due to H_2O molecules with different orientations and H-bonding configurations. The integral intensities of the H_{H2O} peaks at 1.2 Å and 4.3 Å are approximately twice those of the associated O_{H2O} peaks at 1.7 Å and 3.8 Å. This ratio implies that the H_2O molecules located at these positions have both their H_{H2O} atoms pointed towards the nearest hectorite surface and are predominantly donating two H-bonds to the O_b. In contrast, the H_{H2O} peaks at 1.7 Å and 3.8 Å are ~1 Å from the O_{H2O} peak at 2.75 Å, indicating that these H_2O molecules are oriented with one of their H_{H2O} pointed towards the basal surface at any moment in time, with the other pointing approximately parallel to the basal surface. The integral intensity of the O_{H2O} peak at 2.75 Å is ~4 times greater than that of the Ca^{2+} ions sharing approximately the same plane and also the other O_{H2O} peaks. This distribution

suggests that the H_2O molecules at 2.75 Å are in a square planar coordination around the Ca^{2+}. This distribution is very similar to the ADPs of Ca^{2+} and H_2O in the mono-layer hydrate of montmorillonite, which also has a similar H_2O/Ca^{2+} ratio of 6.0.[21, 53]

The ADPs of the complete mono-layer structure are somewhat different from that of the partial mono-layer structure (Figure 3b). The Ca^{2+} distribution shows two peaks for Ca^{2+} centered at 2.8 Å and 3.9 Å, each 2.8 Å from the nearest basal surface at 0.0 Å and 6.7 Å. These distances indicate that the Ca^{2+} ions are adsorbed in inner-sphere (IS) coordination by the O_b of only the closest surface and are in outer sphere (OS) coordination by the opposite surface. Despite the difference in Ca^{2+} distribution, the ADPs of H_2O are generally similar to those of the partial mono-layer structure and are characterized by four and five peaks for O_{H2O} and H_{H2O}, respectively. As for the partial mono-layer structure, the intensities of the H_{H2O} peaks nearest to the basal surfaces are twice those of O_{H2O} peaks closest to the surfaces, indicating that both of the H_{H2O} of the H_2O molecules at these distances point towards the hectorite surface. In parallel, the integral intensities of the H_{H2O} peaks at 1.7 Å and 3.5 Å and the O_{H2O} peak at 2.7 Å are similar, and the distances between them are ~1 Å. These values clearly suggest that the H_2O molecules at distances 2.7 Å from the basal surface are arranged with one H_{H2O} atom pointed towards the basal surface and the other in the mid-plane of the interlayer.

The Ca^{2+} ADPs of the bi-layer hydrate and the external basal surface show a peak centered at distances ~4.0 Å from the hectorite substrate surface (Figure 3c and 3d). This distance clearly indicates that the Ca^{2+} ions are in only OS coordination by all the O_b. Recent experimental ^{43}Ca NMR studies of Ca-hectorite show that the spectra of bi-layer hydrates and samples saturated with H_2O are very similar.[24, 25] The simulation results here support the interpretations of those experimental data that Ca^{2+} is located within 5 Å of the interlayer and external basal surfaces as

OS complexes. In addition, the O_{H2O} ADPs in the near surface regions (z < ~5 Å) for bi-layer hydrate and on the external basal surface are very similar. The adsorption distances indicate the existence of two different types of H_2O molecules as described for the monolayer hydrate. Although there are 20% fewer H_2O molecules in the bi-layer hydrate of hectorite compared to the same structure of montmorillonite, the ADPs are very similar, except near the mid-plane of the interlayer (3.5 – 4.5 Å), where the intensity of the H_2O distribution is greater for montmorillonite due to its larger water content.[21, 53]

In contrast, beyond 5 Å on the external basal surface, there are few Ca^{2+} ions, and O_{H2O} and H_{H2O} show small oscillations extending to ~10.0 Å. Further from the surface, the O_{H2O} and H_{H2O} distributions are similar to those in bulk water, as observed in previous MD modeling studies.[18,40,42,43,62-65] In addition, the near surface H_2O molecules (z < 6 Å) have a different structural distribution than the bulk water, consistent with experimental observations on proximity-restricted H_2O molecules.[24, 25, 27]

For Na-hectorite, Na^+ is in IS coordination by O_b in the mono-layer hydrate and in OS coordination in the bi-layer hydrate, the same as for Ca^{2+} here. The distributions of H_2O molecules in the Na-hectorites are, however, very different, with only one of their H_{H2O} atoms pointing towards surface O_b atoms.[41] On the external surfaces of Na-hectorite, a small fraction (4%) of Na^+ ions are adsorbed in IS coordination, with the others in OS coordination (53%) or detached from the surface (43%), in contrast to the exclusive OS coordination of Ca^{2+} here.[42] In contrast to both these ions, Cs^+ occurs in IS coordination in hectorite interlayers and on its external surfaces irrespective of the hydration state, reflecting its small hydration energy.[43]

Radial Distribution Functions and Running Coordination Numbers

The radial distribution functions (RDFs) and corresponding running coordination numbers (RCNs) for Ca^{2+} - O_{H2O} and Ca^{2+} - O_b pairs in the three modeled interlayer hydration states and on the external basal surface confirm the structural interpretations from the ADPs and provide more detail about the Ca^{2+} and O_{H2O} coordination environments (Figures 4a-4b). Irrespective of the hydration state, the mean interatomic distance between Ca^{2+} and O_{H2O} is ~2.5 Å, similar to the value in bulk solution (Figure 4a).[78-80] The mean interatomic distance between Ca^{2+} and O_b is ~2.7 Å for IS coordination in the partial and complete mono-layer structures and ~4.7 Å for OS coordination in the bi-layer structure and on the external surface (Figure 4b). The values are generally similar to the nearest neighbor (NN) environments in Ca-montmorillonite and Na-hectorite.[21,41,53] For Ca-hectorite, the total RCN of Ca^{2+} is always in the range of 7.0-8.0, but the distribution between H_2O and O_b is different at different hydration states. For the partial mono-layer hydrate structure, the NN coordination of Ca^{2+} consists of 5.0 H_2O and 2.0 O_b (one from each basal surface), whereas it is 6.0 H_2O and 1.0 O_b for the complete mono-layer structure. The coordination with 1.0 O_b in the latter case confirms the suggestion from the ADP that Ca^{2+} ions are adsorbed at IS sites on one hectorite surface but in OS sites on the opposite surface. Similar ranges of RCN values have been reported for Ca-montmorillonite at different H_2O contents and are in excellent agreement with our results.[53]

For the bi-layer hydrate of Ca-hectorite and on its external surface, Ca^{2+} is always coordinated by 8.0 H_2O molecules and 0.0 O_b atoms, consistent with exclusively OS coordination under these conditions. These results are consistent with the ADP results and are also in good agreement with previous simulations of Ca-montmorillonite.[53] The changes in Na^+ coordination by O_b and O_{H2O} in Na-hectorite with increasing interlayer hydration are generally similar to those for Ca-hectorite.[41,53]

Planar Atomic Density Distributions

The planar atomic density distributions (PADDs, also known as atomic probability density maps) on the interlayer and external basal Ca-hectorite surfaces confirm the interpretations of the ADPs discussed above and the analysis of the interfacial H-bonding structure (see Supporting Information). They provide additional detail about the spatial distribution of H_2O molecules and Ca^{2+} ions in the interlayers. The PADDs vary significantly with hydration state (Figures 5a-5e). Because the environments with respect to both sides of the interlayer are the same, these figures illustrate only one surface.

For the partial mono-layer hydration state, the Ca^{2+} ions are adsorbed above one O_b atom from each surface in IS coordination as inferred from the ADPs above (Figure 5a). In addition, each Ca^{2+} ion is coordinated by one H_2O molecule located at the center of a ditrigonal cavity from each surface (illustrated in Figure 5) and 3 H_2O molecules located near the mid-plane of the interlayer z = 2.2 and 3.4 Å with the total coordination of 7, consistent with our RCN values. The H_2O molecules at the center of ditrigonal cavities are adsorbed at distances of z < 2.2 Å from the surface and have both their H_{H2O} atoms donating H-bonds to O_b (Figures 5a and S2). In contrast, the H_2O molecules near the mid-plane are coordinated to O_b atoms through one of their hydrogen atoms at any instant. The compactness of the atomic density contours of individual O_{H2O} and H_{H2O} located in the center of the ditrigonal cavities clearly indicates that these molecules are strongly immobilized on the ns time scale and there is little H-bonding between H_2O molecules, in good agreement with our H-bonding interpretations (See Supporting Information).

The PADDs for the complete mono-layer structure (Figure 5b) show that the Ca^{2+} ions are in IS coordination with respect to one nearest basal surface and in OS coordination with respect to

the other, as inferred from the ADPs above. For instance, the Ca^{2+} ions at z = 2.5-3.5 Å are IS-coordinated with respect to the surface at z = 0 Å and OS-coordinated with respect to the opposite surface at z = 6.7 Å. Figure S3 depicts the relationships of Ca^{2+} ions located at z distances between 3.5-4.5 Å. These Ca^{2+} are in IS coordination with respect to the hectorite surface at z = 6.7 Å and coordinated by the H_2O molecules (z < 2.2 Å), closest to the opposite basal surface at z = 0.0 Å. Each of the Ca^{2+} ions are coordinated by 3 H_2O molecules from each hectorite surface, for a total of 7, consistent with RDF results (Figure 5b). The 3 H_2O molecules per surface are distributed around the Ca^{2+} ions in the following manner. One H_2O molecule is located at the center of a ditrigonal cavity with both H_{H2O} atoms donating H-bonds to the surface, as in Figure S3 (z < 2.2 Å). The two others are adsorbed above O_b atoms and donate only one H-bond to the surface (2.2 < z < 3.4 Å). The same argument can be extended for the 3 other H_2O molecules belonging to the upper surface. As for the partial mono-layer structure, the dense contours of all H_2O molecules around their adsorption sites imply significant immobilization of these molecules and little H-bonding interaction among themselves, in good accordance with our H-bonding interpretation (See Supporting Information).

For the bi-layer hydrate, the PADDs of the Ca^{2+} ions and H_2O molecules close to the basal surface (z < 2.2 Å) show very little correlation (Figure 5c). These H_2O molecules do not coordinate the Ca^{2+} ions but are adsorbed at the centers of neighboring ditrigonal cavities and exhibit greater rotational mobility than in the mono-layer hydrates, as demonstrated by the dispersed contours for H_{H2O}. The PADDs for O_{H2O} and associated H_{H2O} at 2.2 < z < 3.3 Å show that there are four H_2O molecules of this type coordinating each Ca^{2+} ion in the nearest neighbor shell (Figure S4). As for the complete mono-layer structure, these H_2O molecules donate one H-bond to the surface O_b and one to an O_{H2O} in the same plane. Thus, the interlayer Ca^{2+} ions are coordinated by eight H_2O

molecules, four associated with each surface, in excellent agreement with RDF results described above. These eight molecules are arranged in a square antiprism rather than a cube (Figure 5d).

Unlike bi-layer hydrate, the Ca^{2+} ions on the exterior basal surfaces of hectorite are in OS coordination bridged to the surface through H_2O molecules at $z < 2.2$ Å, which are adsorbed at the center of ditrigonal cavities and are coordinated to the O_b by both H_{H2O} (Figure 5e). However, the H_2O molecules at $2.2 < z < 3.3$ Å also participate in the first coordination shell of Ca^{2+} similar to the comparable molecules in the bi-layer hydrate. H_2O molecules farther from the surface complete the hydration shell of Ca^{2+} ions (Figure S5). Again, all features of PADDs are in good agreement with the H-bonding interpretation and with recent simulation studies of Ca-montmorillonite in showing strong coordination of the Ca^{2+} ions by H_2O at all hydration states.[53]

Water Diffusion

Many MD simulations have shown that the diffusion coefficients in clay interlayers are significantly lower than in bulk solution or on the exterior surfaces, even though they increase with increasing interlayer hydration.[21, 43, 53] Our results for H_2O diffusion in Ca-hectorite are similar (Table 2). Recent MD simulation studies of Ca-montmorillonite yield values of ~1×10^{-10} m^2/s for H_2O in the mono-layer hydrate and ~2.5×10^{-10} m^2/s for the bi-layer hydrate,[53] and our results are in excellent agreement with these values. The calculated diffusion coefficients of H_2O molecules in Na-hectorite are 0.2×10^{-10} m^2/s and 4.84×10^{-10} m^2/s for the mono- and bi-layer hydrates, respectively.[41] Neutron scattering experiments have reported H_2O diffusion coefficients in Na-hectorite of 2.8×10^{-10} m^2/s (mono-layer hydrate) and 7.7×10^{-10} m^2/s (bi-layer hydrate).[34, 35] The values reported here for Ca-hectorite are lower than in Na-hectorite, except for the mono-layer hydrate. This is because the larger hydration energy of Ca^{2+} relative to Na^+ keeps the H_2O

molecules more tightly bound to Ca^{2+}, resulting in the decreased mobility. The lower mobility of H_2O molecules in the mono-layer structure of Na-hectorite may be due to the slightly smaller interlayer spacing (~11.8 Å) when compared to Ca-hectorite (~12.3 Å) and to the smaller H_2O/cation ratio, which results in a larger fraction of the water molecules being coordinated to the cation. The diffusion coefficients of interlayer H_2O in Cs-hectorite are significantly larger than for Ca-hectorite, as expected from the smaller hydration energy of Cs^+.[20,43,44] However, the H_2O diffusion coefficients on the external surfaces of hectorite do not depend significantly on the counterion and are all ~30.0×10^{-10} m^2/s.[42,43] This value is in excellent agreement with the computed self-diffusion coefficients of bulk SPC water.[42, 43, 72]

Site Residence Times

The dynamical behavior of the coordination structure around metal cations in clay interlayers and the coordination of H_2O to basal O_b atoms can be further quantitatively characterized by computing the mean residence times of H_2O molecules and surface O_b atoms in the first coordination shell of the metal cation. For Ca-hectorite, the values of the mean intermittent $c(t)$ residence times for the Ca^{2+} - H_2O, Ca^{2+} - O_b and H_2O – O_b pairs are all of the order of 1 – 30 ns, are slightly shorter for the complete mono-layer structure than for the partial mono-layer structure, and are an order of magnitude shorter for the bi-layer structure than for either of the mono-layer structures. The continuous residence times, $C(t)$, show similar trends, but are substantially shorter than the intermittent residence times. For the partial and complete mono-layer structures, the mean residence times of H_2O molecules in the Ca^{2+} NN shell are ~2 (intermittent) and ~5 (continuous) times longer than those of O_b atoms around Ca^{2+} ions. This result is consistent with the large hydration energy of Ca^{2+}. In contrast, the H_2O and O_b residence times in NN coordination to Cs^+ are much shorter than Ca-hectorite, and Cs^+ - H_2O residence times are shorter

than the Cs^+ - O_b residence times, again due to the smaller hydration energy of Cs^+.[43] For Ca-hectorite, the residence times for H_2O–O_b coordination are about an order of magnitude shorter than for H_2O-Ca^{2+} coordination, reflecting the fact that H-bonding interactions are weaker than the dominant Coulombic interactions in this system. The H_2O-O_b residence times for the mono-layer structures of Ca-hectorite are approximately seven times larger than for Cs-hectorite.[43] This is probably due to the Ca^{2+} ions being adsorbed above O_b atoms and the H_2O molecules at the center of ditrigonal cavities for Ca-hectorite, in contrast to the opposite coordination in Cs-hectorite.[43] This difference affects the residence times, because the H_2O molecules in the ditrigonal cavities donate two H-bonds to the O_b instead of one, and these H_2O molecules also contribute to the nearest coordination shell of Ca^{2+} (see the PADD results in Figure 5a, 5b). The long residence times at low water content recently reported for Ca-montmorillonite are in good agreement with our results.[53]

The shorter residence times in the bi-layer hydrate reflect the increased probability for H_2O molecules to exchange between the nearest and next nearest neighbor coordination shells of Ca^{2+} as water content increases and parallels the increase in the diffusion rates. Decreased steric restrictions and an increasing number of relatively weak H-bonds may both play important roles in the determination of residence times. There are no values for Ca^{2+}-O_b residence times for the bi-layer hydrate, because Ca^{2+} ions are adsorbed on OS sites at this hydration state.

CONCLUSIONS

Classical MD simulations of Ca-hectorite with a wide range of hydration states (0-35 H_2O/Ca^{2+}) using a new hectorite model with a disordered distribution of isomorphic Li^+/Mg^{2+} substitutions in the octahedral sheet have been performed to investigate the structure, dynamics

and energetics of the interlayer galleries and external surfaces of smectite materials exchanged with Ca^{2+}. The simulated interlayer spacings are in good agreement with experimental XRD measurements.[24,25,27] The analysis of the calculated hydration and immersion energies suggests the existence of three well defined hydration states corresponding to a partially filled mono-layer hydrate, a complete mono-layer hydrate, and a bi-layer hydrate. All these hydration states are potentially realizable at different RH conditions. The hydration energies are always lower than the energy of the bulk SPC water model used, suggesting that further expansion to higher hydration levels is possible, as recently observed experimentally.[25] The values of the hydration energies of Ca-hectorite are significantly more negative than for Na- and Cs-hectorite at all hydration states.[41,43] The hydration energy sequence ($Ca^{2+} > Na^{+} > Cs^{+}$) illustrates well the role of ion hydration energy in controlling the structure and energetics of the interlayer galleries of smectite materials. The calculated basal spacing and hydration energetics of Ca-hectorite are in good agreement with recent simulation studies of Ca-montmorillonite.[21,53]

Ca^{2+} ions are adsorbed in inner sphere coordination by the basal surfaces in the partial and complete mono-layer structures but in only outer sphere coordination in the bi-layer hydrate and on the external (001) surface. Irrespective of the hydration state, H_2O molecules occur in two different structural environments: (i) in the center of ditrigonal cavities donating two H-bonds to the O_b atoms of the basal surface, and (ii) above an O_b atom and H-bonded to it by one of its H_{H2O} atoms. In the partially filled and complete mono-layer hydrates and the bi-layer hydrate, H_2O molecules in nearest neighbor coordination to Ca^{2+} exhibit only weak H-bonding interactions among themselves. Self-diffusion coefficients of H_2O molecules in the interlayer galleries are an order of magnitude lower than on the external surface and are approximately a factor of 2 larger for the bi-layer hydrate than the two mono-layer hydrates, illustrating the effects of the bounding

basal surfaces. The residence times of H_2O and O_b atoms in nearest neighbor coordination to Ca^{2+} ions are longer for the mono-layer hydrates than the bi-layer hydrate, paralleling the diffusion results. The site residence times for Ca-hectorite are significantly longer than for Cs-hectorite, clearly showing that cations with low hydration energies and large ionic radii prefer to be coordinated to the basal oxygen atoms of the clay surface under ambient conditions.

ACKNOWLEDGMENTS

All the calculations in this work were performed using computational resources at the National Energy Research Scientific Computing Center, which is supported by the Office of Science of the U.S. Department of Energy under ECARP No. m1649. This research is supported by U.S. Department of Energy Office of Basic Energy Sciences to Michigan State University under the grant DE-FG02-08ER15929 (R. J. Kirkpatrick, P.I.) and by U.S. DOE grant DE-FG0210ER16128 at Alfred University (G.M. Bowers, P.I.). AGK acknowledges the support of the industrial chair "Storage and Disposal of Radioactive Waste" at the Ecole des Mines de Nantes, funded by ANDRA, Areva, and EDF.

ASSOCIATED CONTENT

Supporting Information. Details of H-Bonding Structure and planar atomic density distributions (PADDs) of near surface adsorbed H_{H2O} for partial, complete monolayer and bi-layer hydrate, schematic representation of Ca^{2+} on the external basal surface.

Notes

The authors declare no competing financial interest.

REFERENCES

1. Sposito, G.; Skipper, N. T.; Sutton, R.; Park, S.; Soper, A. K.; Greathouse, J. A. Surface Geochemistry of Clay Minerals. *Proc. Natl. Acad. Sci.* **1999**, *96*, 3358-3364.
2. Yuan, G. D.; Theng, B. K. G.; Churchman, G. J.; Gates, W. P. Clays and Clay Minerals for Pollution Control. Handbook of Clay Science, 2006, 1, 625-675.
3. Higgins, J. M.; Polcik, M.; Fukuma, T.; Sader, E. J.; Nakayama, Y; Jarvis, P. S. Structured Water Layers Adjacent to Biological Membranes. *Biophys. Journal* **2006**, *91*, 2532-2542.
4. Benson, M. S.; Cole, R. D. CO_2 Sequestration in Deep Sedimentary Formations. *Elements* **2008,** 4, 325-331.
5. Lackner, K. S. A Guide to CO_2 Sequestration. *Science* **2003,** *300*, 1677-1678.
6. Marklund, L.; Simic, E.; Worman,A.; Dverstorp, B. The Impact of Different Geological Parameters on Transport of Radionuclides. In Proceedings of 2006 International High-Level Radioactive Waste Management Conference; American Nuclear Society, Las Vegas, NV, 36-373.
7. Bodvarsson, G. S.; Boyle, W.; Patterson, R.; Williams, D. Overview of Scientific Investigations at Yucca Mountain – The Potential Repository for High-Level Nuclear Waste. *J. Contam. Hydrol.* **1999**, *38*, 3-24.
8. Long, J. C. S.; Ewing, R. C. Yucca Mountain: Earth-Sciences Issues at a Geological Repository for High-Level Nuclear Waste. *Annu. Rev. Earth Planet Sci.* **2004**, 32, 363-401.
9. Vieillard, P.; Ramirez, S.; Bouchet, A, A.; Cassagnabere, A.; Meunier, A.; Jacquot, E. Alteration of the Callovo-Oxfordian Clay from Meuse-Haute Marne Underground Laboratory (France) by Alkaline Solution: II Modeling of Mineral Reactions. *Appl. Geochem.* **2004**, *19*, 1699-1709.
10. Nones, J.; Riella, H. G.; Trentin, A. G.; Nones, J. Effects of Bentonite on Different Cell Types: A Brief Review. *Appl. Clay. Sci*. **2015**, *105*, 225-230.
11. Dawson, J. I.; Oreffo, R. O. C. Clay: New Opportunities for Tissue Regeneration and Biomaterial Design. *Adv. Mater*. **2013**, *25*, 4069-4086.
12. Raous, S.; Echevarria. G.; Sterckeman, T.; Hanna, K.; Thomas, F.; Martin, E. S.; Becquer, T. Potentially Toxic Metals in Ultramafic Mining Materials: Identification of the Main Bearing and Reactive Phases. *Geoderma*. **2013**, *192*, 111-119.
13. Fujita, S.; Bhanage, B. M.; Ikushima, Y.; Shirai, M.; Torii, K.; Arai, M. Chemical Fixation of Carbon dioxide to Propylene Carbonate Using Smectite Catalysts with High Activity and Selectivity. *Catalysis Lett*. **2002**, *79*, 1-4.
14. Rotenberg, B.; Marry, V.; Vuilleumier, R.; Malikova, N.; Simon, C.; Turq, P. Water and Ions in Clays: Unraveling the Interlayer/Micropore Exchange using Molecular Dynamics. *Geochim. Cosmochim. Acta* **2007,** *71*, 5089-5101.
15. Bourg, I. C.; Sposito, G.; Bourg, A. C. M. Tracer Diffusion in Compacted, Water-Saturated Bentonite. *Clays Clay Miner.* **2006**, *54*, 363-374.

16. Ngouana, W. B. F.; Kalinichev, A. G. Structural Arrangements of Isomorphic Substitutions in Smectites: Molecular Simulation of the Swelling Properties, Interlayer Structure and Dynamics of Hydrated Cs-Montmorillonite Revisited with New Clay Models. *J. Phys. Chem. C* **2014**, *118*, 12758-12773.

17. Liu, X.; Lu, X.; Wang, R.; Zhou, H. Effects of Layer-Charge Distribution on the Thermodynamic and Microscopic Properties of Cs-Smectite. *Geochim. Cosmochim. Acta* **2008**, *72*, 1897-1847.

18. Wang, J.; Kalinichev, A. G.; Kirkpatrick, R. J. Effects of Substrate Structure and Composition on the Structure, Dynamics and Energetics of Water at Mineral Surfaces: A Molecular Dynamics Modeling Study. *Geochim. Cosmochim. Acta* **2006,** *70*, (3), 562-582.

19. Sposito, G.; Park, S. H.; Sutton, R. Monte Carlo Simulation of the Total Radial Distribution Function of Interlayer Water in Sodium and Potassium Montmorillonites. *Clays Clay Miner.* **1999**, *47*, 192-200.

20. Sutton, R.; Sposito, G. Animated Molecular Dynamics Simulations of Hydrated Caesium-Smectite Interlayers. *Geochem. Trans.* **2002**, *3*, 73-80.

21. Teich-McGoldrick, S. L.; Greathouse, J. A., Colon, C. F.; Cygan, R. T. Swelling Properties of Montmorillonite and Beidellite Clay Minerals from Molecular Simulation: Comparison of Temperature, Interlayer Cation, and Charge Location Effects. *J. Phys. Chem. C* **2015**, *119*, 20880-20891.

22. Bowers, G. M.; Singer, J. W.; Bish, D. L.; Kirkpatrick, R. J. Alkali Metal and H_2O Dynamics at the Clay/Water Interface. *J. Phys. Chem. C* **2011**, *115*, 23395-23407.

23. Weiss, C. A.; Kirkpatrick, R. J.; Altaner, S. P. The Structural Environments of Cations Adsorbed onto Clays – Cs 133 Variable Temperature MAS NMR Spectroscopic Study of Hectorite. *Geochim. Cosmochim. Acta* **1990**, *54*, 1655-1669.

24. Bowers, G. M.; Singer, J. W.; Bish, D. L.; Kirkpatrick, R. J. Structure and Dynamical Relationships of Ca^{2+} and H_2O in Smectite/^2H_2O Sytems. *Ameri. Mineral*. 2014, *99*, 318-331.

25. Reddy, U. V. ; Bowers, G. M.; Loganathan, N.; Bowden, M. ; Yazaydin, A. O.; Kirkpatrick, R. J. Water Structure and Dynamics in Smectites: ^2H NMR Spectroscopy of Mg, Ca, Sr, Cs and Pb-Hectorite. *J. Phys. Chem. C* **2016**, *120*, 8863-8876.

26. Bowers, G. M.; Bish, D. L; Kirkpatrick, R. J. H_2O and Cation Structure and Dynamics in Expandable Clays: ^2H and ^{39}K NMR Investigations of Hectorite. *J. Phys. Chem. C* **2008**, *112*, 6430-6438.

27. Ferguson, B. O.; Arey, B.; Varga, T.; Burton, S.; Bowden, M.; Argersinger, H. E.; Kirkpatrick, R. J.; Bowers, G. M. X-ray Diffraction and Helium ion and Electron Microscopy of Smectite-Natural Organic Matter Composites. *Clays Clay Minerals* **(Submitted)**

28. Karmous, M. S.; Ben Rhaiem, H.; Robert, J. L., Lanson, B.; Amara, A. B. H. Charge Location Effect on the Hydration Properties of Synthetic Saponite and Hectorite Saturated by Na^+, Ca^{2+} Cations: XRD Investigation. *Appl. Clay. Sci*. **2009**, *46*, 43-50.

29. Karmous, M. S.; Oueslati, W.; Ben Rhaiem, H.; Robert, J. L., Amara, A. B. H. Simulation of the XRD Patterns, Structural Properties of a Synthetic Na-Hectorite Exchange Cu^{2+} and Ca^{2+}. *Z. Kristallogr*. **2007**, *26*, 503-508.

30. Kalo, H.; Milius, W.; Breu, J. Single Crystal Structure Refinement of One- and Two-Layer Hydrates of Sodium Fluorohectorite. *RSC Adv.* **2012**, *2*, 8452-8459.

31. Porion, P.; Warmont, F.; Faugere, A. M.; Rollet, A-L.; Dubois, E.; Marry, V.; Michot, L. J.; Delville, A. ^{133}Cs Nuclear Magnetic Resonance Relaxometry as a Probe of the Mobilty of Cesium Cations Confined within Dense Clay Sediments. *J. Phys. Chem. C* **2015**, *119*, 15360-15372.

32. Tenorio, R. P.; Alme, L. R.; Engelsberg, M.; Fossum, J. O.; Hallwass, F. Geometry and Dynamics of Intercalated Water in Na-Fluorohectorite Clay Hydrates. *J. Phys. Chem C* **2008**, *112*, 575-580.

33. Marry, V.; Malikova, N.; Cadene, A.; Dubois, E.; Durand-Vidal, S.; Turq, P.; Breu, J.; Longeville, S.; Zanotti, J. M. Water Diffusion in a Synthetic Hectorite by Neutron Scattering – Beyond the Isotropic Translational Model. *J. Phys.: Condens. Matter* **2008**, *20*, 104205.

34. Marry, V.; Dubois, E.; Malikova, N.; Durand-Vidal, S.; Longeville, S.; Breu, J. Water Dynamics in Hectorite Clays: Influence of Temperature Studied by Coupling Neutron Spin Echo and Molecular Dynamics. *Environ. Sci. Technol.* **2011**, *45*, 2850-2855.

35. Malikova, N.; Cadene, A.; Dubois, E., Marry, V.; Durand-Vidal, S.; Turq, P.; Breu, J.; Longeville, S.; Zanotti, J. M. Water Diffusion in a Synthetic Hectorite Clay Studied by Quasi-Elastic Neutron Scattering. *J. Phys. Chem C* **2007**, *111*, 17603-17611.

36. Skipper, N. T.; Lock, P. A.; Titiloye, J. O.; Swenson, J.; Mirza, Z.; Howells, W. S.; Alonso, F. F. The Structure and Dynamics of 2-Dimensional Fluids in Swelling Clays. *Chem. Geol*. **2006**, *230*,183-196.

37. Rotenberg, B.; Marry, V.; Malikova, N.; Turq, P. Molecular Simulation of Aqueous Solutions at Clay Surfaces. *J. Phys. Condens. Matter* **2010**, *22*, 284114.

38. Boek, E. S.; Sprik, M. Ab Initio Molecular Dynamics Study of the Hydration of a Sodium Smectite Clay. *J. Phys. Chem B* **2003,** *107*, 3251-3256.

39. Greathouse, J. A.; Cygan, R. T. Water Structure and Aqueous Uranyl (VI) Adsorption Equilibria onto External Surfaces of Beidellite, Montmorillonite and Pyrophyllite: Results from Molecular Simulations. *Environ. Sci. Technol.* **2006**, *40*, 3865-3871.

40. Yazaydin, A. O.; Bowers, G. M.; Kirkpatrick, R. J. Molecular Dynamics Modeling of Carbon dioxide, Water and Natural Organic Matter in Na-Hectorite. *Phys. Chem. Chem. Phys*. **2015**, *17*, 23356-23367.

41. Morrow, C. P.; Yazaydin, A. O.; Krishnan, M.; Bowers, G. M.; Kalinichev, A. G.; Kirkpatrick. R. J. Structure, Energetics and Dynamics of Smectite Clay Interlayer Hydration: Molecular Dynamics and Metadynamics Investigation of Na-Hectorite. *J. Phys. Chem. C* **2013**, *117*, 5172-5187.

42. Greathouse, J. A.; Hart, D. B.; Bowers, G. M.; Kirkpatrick, R. J.; Cygan, R. T. Molecular Simulation of Structure and Diffusion at Smectite-Water Interfaces: Using Expanded Clay Interlayers as Model Nanopores. *J. Phys. Chem. C* **2015**, *119*, 17126-17136.

43. Loganathan, N.; Yazaydin, A. O.; Bowers, G. M.; Kalinichev, A. G.; Kirkpatrick, R. J. Structure, Energetics and Dynamics of Cs^+ and H_2O in Hectorite: Molecular Dynamics Simulations with a Unconstrained Substrate Surface. *J. Phys. Chem. C,* DOI 10.1021/acs.jpcc.6b01016.

44. Sutton, T.; Sposito, G. Molecular Simulation of Interlayer Structure and Dynamics in 12.4Å Cs-Smectite Hydrates. *J. Coll. Interf. Sci*. **2001**, *237*, 174-184.

45. Hartzell, C. J.; Cygan, R. T.; Nagy, K. L. Molecular Modeling of the Tributyl Phosphate Complex of Europium Nitrate in the Clay Hectorite. *J. Phys. Chem. A* **1998**, *102*, 6722-6729.

46. Dore, J. Structural Studies of Water in Confined Geometry by Neutron Diffraction. *Chem. Phys*. **2000**, *258*, 327.

47. Smith, D. E. Molecular Computer Simulations of the Swelling Properties and Interlayer Structure of Cesium Montmorillonite. *Langmuir* **1998**, *14*, 5959-5967.

48. Hensen, E. J. M.; Smit, B. Why Clays Swell. *J. Phys. Chem. B* **2002**, *106*, 12664-12667.

49. Calvet, R. Hydration of Montmorillonite and Diffusion of Exchangeable Cations. 1. Hydration of Montmorillonite Saturated by Monovalent Cations. *Ann. Agron.* **1973**, *24*, 77-133.

50. Salles, F.; Douillard, J-M.; Bildstein, O.; Ghazi, S. E.; Perlot, B.; Zajac, J.; Damme, H. V. Diffusion of Interlayer Cations in Swelling Clays as a Function of Water Content: Case of Montmorillonites Saturated with Alkali Cations. *J. Phys. Chem C* **2015,** *119*, 10370-10378.

51. Salles, F.; Bildstein, O.; Douillard, J-M.; Jullien, M.; Raynal, J.; Damme, H. V. On the Cation Dependence of Interlamellar and Interparticle Water and Swelling in Smectite Clays. *Langmuir* **2010,** *26*, 5028-5037.

52. Berend, I.; Cases, J-M.; Francois, M.; Uriot, J-P.; Michot, L.; Masion, A.; Thomas, F. Mechanism of Adsorption and Desorption of Water Vapor by Homoionic Montmorillonites: 2. The Li^+, Na^+, K^+, Rb^+ and Cs^+ Exchanged Forms. *Clays Clay Miner.* **1995**, *43*, 324-336.

53. Zhang, L.; Lu, X.; Zhou, J.; Zhou, H. Hydration and Mobility of Interlayer Ions of (Na_x, Ca_y)-Montmorillonite: A Molecular Dynamics Study. *J. Phys. Chem. C* **2014**, *118*, 29811-29821.

54. Boulet, P.; Bowden, A. A.; Coveney, P. V.; Whiting, A. Combined Experimental and Theoretical Investigations of Clay Polymer Nano-Composites: Intercalation of Single Bifunctional Organic Compounds in Na^+-Montmorillonite and Na^+-Hectorite Clays for the Design of New Materials. *J. Mater. Chem.* **2003**, *13*, 2540-2550.

55. Bowers, G. M.; Hoyt, D. W.; Burton, S. D.; Ferguson, B. O.; Varga, R.; Kirkpatrick, R. J. In Situ ^{13}C and ^{23}Na Magic Angle Spinning NMR Investigation of Supercritical CO_2 Incorporation in Smectite-Natural Organic Matter Composites. *J. Phys. Chem C* **2014,** *118*, 3564-3573.

56. Kalinichev, A. G.; Iskrenova-Tchoukova, E,; Ahn, W-Y.; Clark, M. M.; Kirkpatrick, R. J. Effects of Ca^{2+} on Supramolecular Aggregation of Natural Organic Matter in Aqueous Solutions: A Comparison of Molecular Modeling Approaches. *Geoderma* **2011**, *169*, 27-32.

57. Bowers, G. M.; Argersinger, H. E.; Reddy, U. V.; Johnson, T. A.; Arey, B.; Bowden, M.; Kirkpatrick, R. J. Integrated Molecular and Microscopic Scale Insight into Morphology and

Ion Dynamics in Ca^{2+}-Mediated Natural Organic Matter Floccs. *J. Phys. Chem. C* **2015**, *119*, 17773-17783.

58. Weiss, C. A.; Kirkpatrick, R. J.; Altaner, S. P. The Structural Environments of Cations Adsobed onto Clays – Cs 133 Variable Temperature MAS NMR Spectroscopic Study of Hectorite. *Geochim. Cosmochim. Acta* **1990**, *54*, 1655-1669.

59. Breu, J.; Seidl, W.; Stoll, A. Disorder in Smectites in Dependence of the Interlayer Cation. Z. *Anorg. Allg. Chem*. **2003**, *629*, 503-515.

60. Malikova, N.; Dubois, E., Marry, V.; Rotenberg, B.; Turq, P. Dynamics in Clays – Combining Neutron Scaterring and Microscopic Simulation. *Z. Phys. Chem* **2010**, *224*, 153-181.

61. Lowenstein, W. The Distribution of Aluminium in the Tetrahedra of Silicates and Aluminates. *Am. Mineral*. **1954**, *39*, 92-96.

62. Wang, J.; Kalinichev, A. G.; Kirkpatrick, R. J.; Cygan, R. T. Structure, Energetics and Dynamics of Water Adsorbed on the Muscovite (001) Surface: A Molecular Dynamics Simulation. *J. Phys. Chem B* **2005,** *109*, 15893-15905.

63. Malani, A.; Ayappa, K. G.; Murad, S. Adsorption Isotherms of Water on Mica: Redistribution and Film Growth. *J. Phys. Chem B* **2009,** *113*, 1058-1067.

64. Loganathan, N.; Kalinichev, A. G. On the Hydrogen Bonding Structure at the Aqueous Interface of Ammonium-Substituted Mica: A Molecular Dynamics Simulation. *Zeitschrift fur Naturforschung* **2013,** *68a*, 91-100.

65. Loganathan, N.; Kalinichev, A. G.(Unpublished results)

66. Plimpton, S. Fast Parallel Algorithms for Short-Range Molecular Dynamics. *J. Comp. Phys.* **1995,** *117*, (1), 1-19.

67. Shinoda, W.; Shiga, M.; Mikami, M. Rapid Estimation of Elastic Constants by Molecular Dynamics Simulations under Constant Stress. *Phys. Rev. B.* **2004,** *69*, 134103.

68. Tuckerman, M. E.; Alejandre, J.; Rendon, R.; Jochim, A. A.; Martyna, G. J. A Liouville-Operator Derived Measure-Preserving Integrator for Molecular Dynamics Simulations in the Isothermal-Isobaric Ensemble. *J. Phys. A: Math. Gen* **2006,** *39*, 5629-5651.

69. Cygan, R. T.; Liang, J.-J.; Kalinichev, A. G. Molecular Models of Hydroxide, Oxyhydroxide and Clay Phases and the Development of a General Force Field. *J. Phys. Chem. B* **2004,** *108*, 1255-1266.

70. Narasimhan, L.; Boulet, P.; Kuchta, B.; Schaef, O.; Denoyel, R.; Brunet, P. Molecular Simulations of Water and Paracresol in MFI Zeolite – A Monte Carlo Study. *Langmuir* **2009**, *25*, 11598-11607.

71. Narasimhan, L.; Kuchta, B.; Schaef, O.; Brunet, P.; Boulet, P. Mechanism of Adsorption of p-cresol Uremic Toxin into Faujasite Zeolites in Presence of Water and Sodium Ions – A Monte Carlo Study. *Micro. Meso. Mat*. **2013**, *173*, 70-77.

72. Teleman, O.; Jonsson, B.; Engstrom, S. A Molecular Dynamics Simulation of a Water Model with Intramolecular Degrees of Freedom. *Mol. Phys*. **1987**, *60*, 193-203.

73. Luzar, A.; Chandler, D. Hydrogen-bond Kinetics in Liquid Water. *Nature* **1996**, *379*, 55-57.

74. Luzar, A. Resolving the Hydrogen Bond Dynamics Conundrum. *J. Chem. Phys*. **2000**, *113*, 10663.

75. Chowdhuri, S.; Chandra, A. Dynamics of Halide Ion-Water Hydrogen Bonds in Aqueous Solutions: Dependence on Ion Size and Temperature. *J. Phys. Chem. B* **2006**, *110*, 9674-9680.

76. Iskrenova-Tchoukova, E.; Kalinichev, A. G.; Kirkpatrick, R. J. Metal Cation Complexation with Natural Organic Matter in Aqueous Solutions: Molecular Dynamics Simulations and Potentials of Mean Force. *Langmuir* **2010**, *26*, 15909-15919.

77. Impey, R. W.; Madden, P. A.; McDonald, I. R. Hydration and Mobility of Ions in Solution. *J. Phys. Chem.* **1983**, *87*, 5071-5083.

78. Koneshan, S.; Rasaiah, J. C.; Lynden-Bell, R. M.; Lee, S. H. Solvent structure, dynamics and the ion mobility in aqueous solution at 25 degrees C *J. Phys. Chem. B* **1998**, *102*, 4193-4204.

79. Ohtaki, H.; Radnai, T. Structure and Dynamics of Hydrated Ions. *Chem. Rev* **1993,** *93*, 1157-1204

80. Aqvist, J. Ion-Water Interaction Potential Derived from Free Energy Perturbation Simulations. *J. Phys. Chem.* **1990**, *94*, 8021-8024.

Table 1. Calculated basal spacings (Å) of dry and hydrated Ca-hectorite compared with experimental values of Ca-hectorite and previous modeling results for Na- and Cs-hectorite and Ca-montmorillonite.

	Dry (Å)	Mono-layer (Å)	Bi-layer (Å)
Ca-hectorite			
This work	9.6	12.3	14.9
Expt.[24, 27]	12.8	12.8	15.1
Expt.[25, 28, 29]	12.9	12.9	15.6
Na-hectorite[41]	9.6	11.8	15.2
Cs-hectorite[43]	10.7	12.4	
Ca-montmorillonite			
Simulation[21]	9.4	12.0	14.6
Simulation[53]	9.4	11.9	15.2

Table 2. Calculated diffusion coefficients of H_2O molecules in the interlayer galleries of Ca-hectorite hydrates and on the external basal surface.

Hydration level	H_2O Diffusion Coefficient ($10^{-10}m^2/s$)
Partial mono-layer	0.91
Complete mono-layer	1.03
Bi-layer	2.54
External Surface	30.72

Table 3. Calculated intermittent and continuous residence times (ns) for the listed atomic pairs in the interlayers of Ca-hectorite.

Hydration state	Ca^{2+} - O_{H2O} (ns)	Ca^{2+} - O_b (ns)	O_{H2O} – O_b (ns)
Intermittent Residence Time (τ_{res}^{I})			
Partial mono-layer	27.4	13.2	2.8
Complete mono-layer	26.2	11.9	2.5
Bi-layer	1.9		0.5
Continuous Residence Time (τ_{res}^{C})			
Partial mono-layer	2.6	0.73	0.58
Complete mono-layer	2.4	0.52	0.38
Bi-layer	0.4		0.04

FIGURE CAPTIONS

Figure 1. Snapshots of the simulated Ca-hectorite system illustrating the disordered distribution of Li^{+}/Mg^{2+} substitution in the octahedral sheet. a) View perpendicular to the clay layers. b) External basal surface viewed parallel to the clay layers along the *xy* direction. Purple balls – octahedral Li^{+}, green balls – octahedral Mg^{2+}, yellow – Si tetrahedra, blue balls – interlayer Ca^{2+} ions, red sticks – O_{H2O}, white sticks – H_{H2O}. For the sake of clarity the structural OH^{-} groups are not shown.

Figure 2. Swelling properties of Ca-hectorite as functions of interlayer water content: a) interlayer basal spacing; b) hydration energy; c) immersion energy. The dashed line in b) indicates the internal energy of the SPC water model used in the simulations. The error bars show the 90% confidence level.

Figure 3. Computed atomic density profiles of O_b (blue), Ca^{2+} (orange), O_{H2O} (red) and H_{H2O} (cyan) in Ca-hectorite as functions of distance from the basal clay surface for: a) the partial mono-layer hydrate; b) the complete mono-layer hydrate; c) the bi-layer hydrate; d) the external hectorite surface.

Figure 4. Radial distribution functions (solid lines) and the corresponding running coordination numbers (dashed lines) for atomic pairs in the interlayers and on the external surface of Ca-hectorites: a) Ca^{2+}-O_{H2O}; b) Ca^{2+}-O_b. Black – partial mono-layer hydrate; red – complete mono-layer hydrate; green – bi-layer hydrate; blue – external (001) surface.

Figure 5. Spatial arrangements of Ca^{2+} ions and H_2O molecules a) pictorial representation of the nearest H_2O molecules coordinating interlayer Ca^{2+} ions in partial monolayer hydrate; b) pictorial representation of the nearest H_2O molecules coordinating interlayer Ca^{2+}

ions in complete monolayer hydrate; c) calculated PADDs of Ca^{2+} and H_2O molecules at $z < 2.2$ Å in bi-layer hydrate; d) pictorial representation of the near surface H_2O molecules coordinating an interlayer Ca^{2+} ion in bi-layer hydrate e) calculated PADDs of Ca^{2+} and H_2O molecules at $z < 2.2$ Å on external basal surface. Color code: O_b – gray, Si – yellow, Ca^{2+} – blue, O_{H2O} – red, H_{H2O} – cyan.

FIGURES

a) 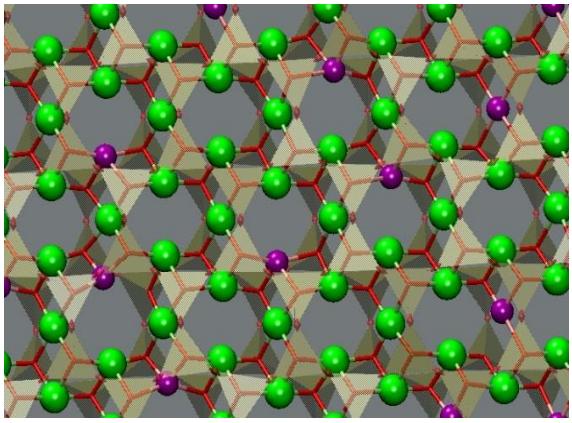 b) 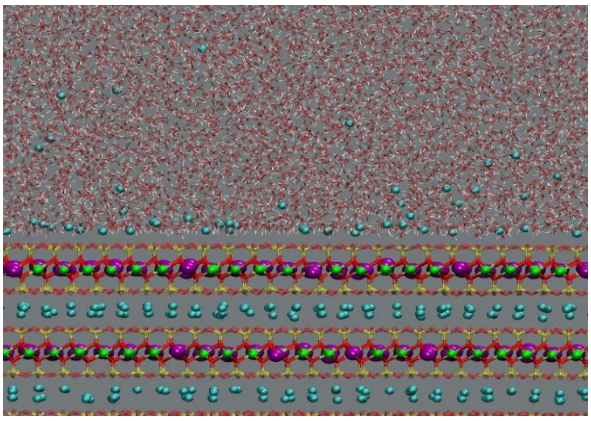

Figure 1. Snapshots of the simulated Ca-hectorite system illustrating the disordered distribution of Li^{+}/Mg^{2+} substitution in the octahedral sheet. a) View perpendicular to the clay layers. b) External basal surface viewed parallel to the clay layers along the *xy* direction. Purple balls – octahedral Li^{+}, green balls – octahedral Mg^{2+}, yellow – Si tetrahedra, blue balls – interlayer Ca^{2+} ions, red sticks – O_{H2O}, white sticks – H_{H2O}. For the sake of clarity the structural OH^{-} groups are not shown.

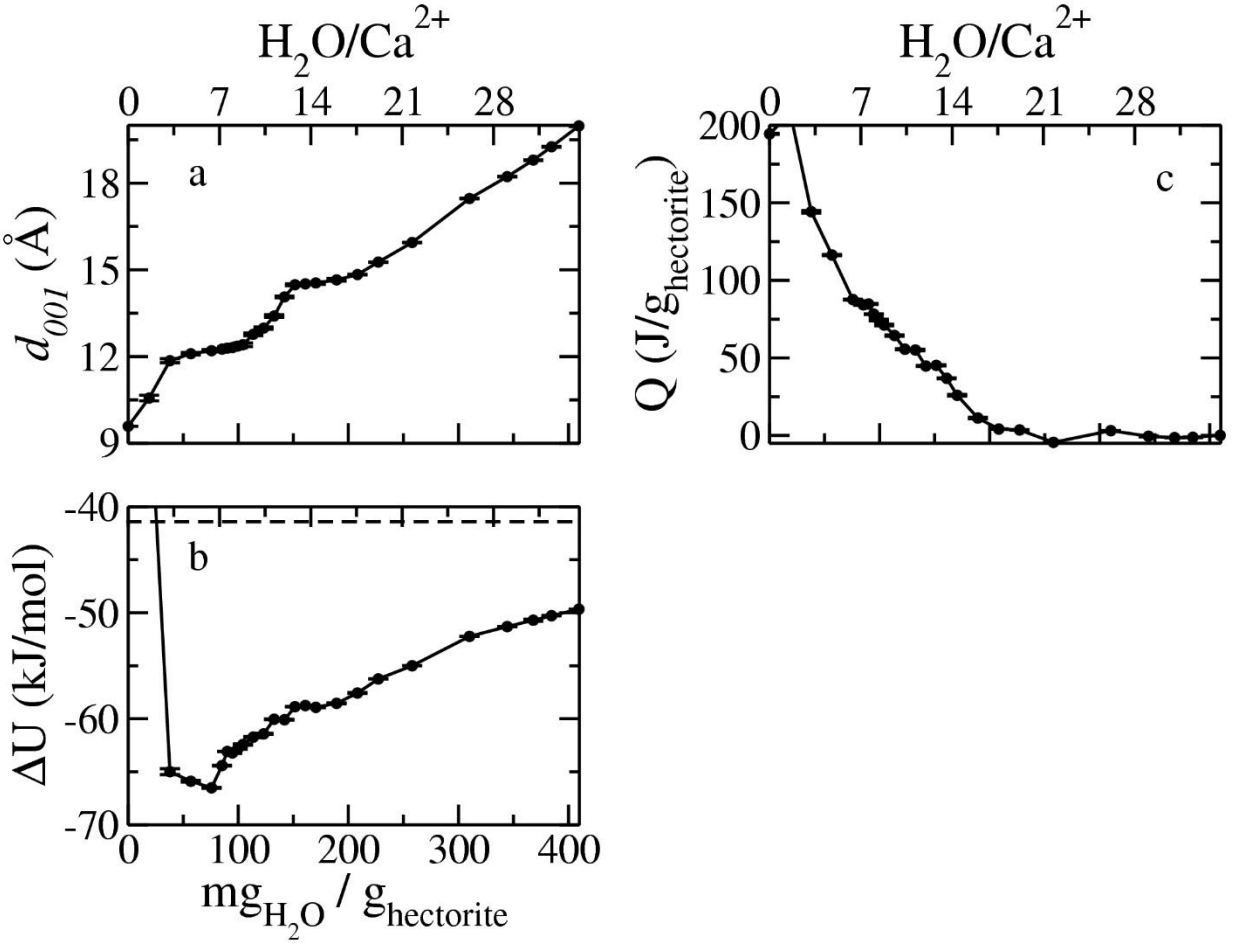

Figure 2. Swelling properties of Ca-hectorite as functions of interlayer water content: a) interlayer basal spacing; b) hydration energy; c) immersion energy. The dashed line in b) indicates the internal energy of the SPC water model used in the simulations. The error bars show the 90% confidence level.

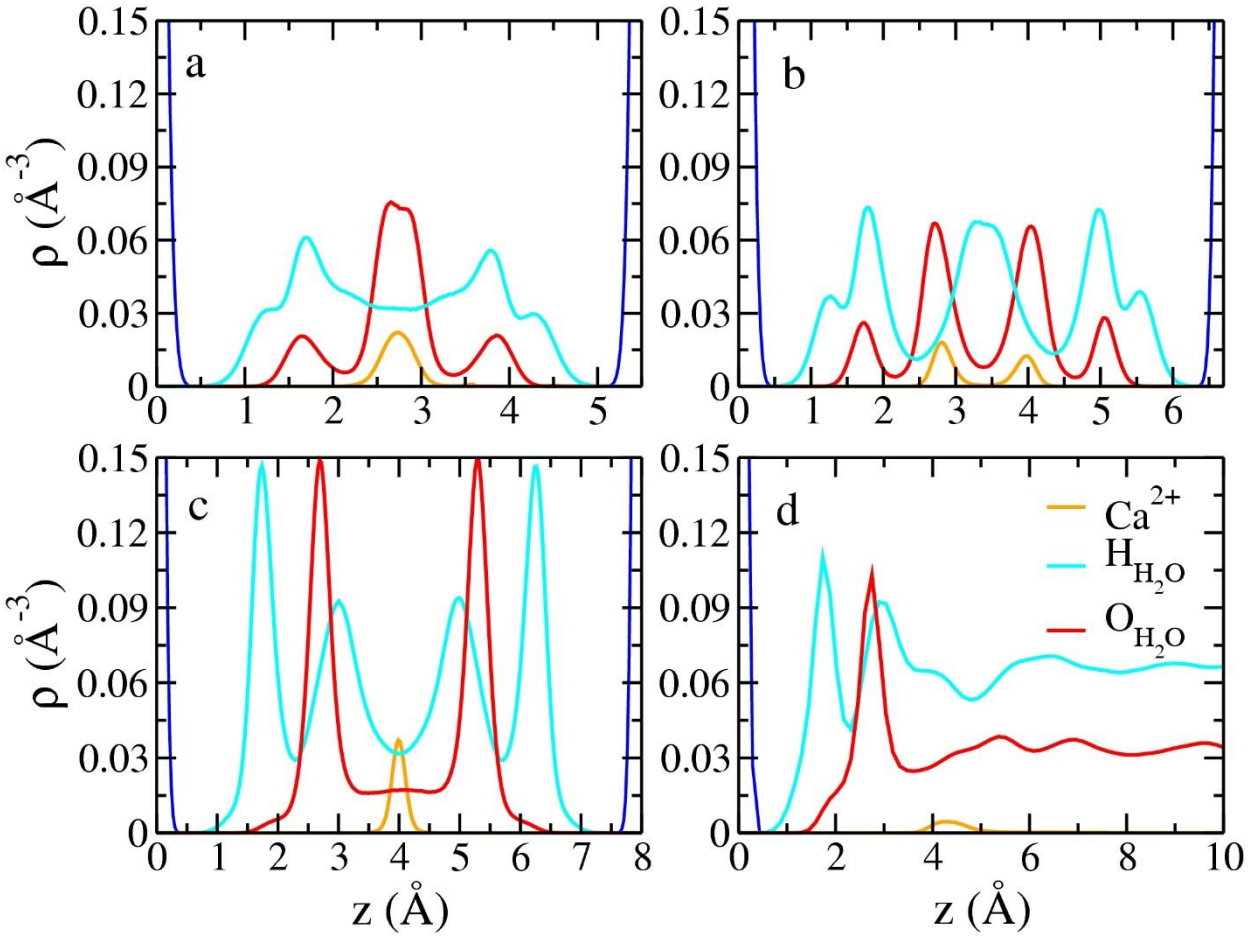

Figure 3. Computed atomic density profiles of O_b (blue), Ca^{2+} (orange), O_{H2O} (red) and H_{H2O} (cyan) in Ca-hectorite as functions of distance from the basal clay surface for: a) the partial mono-layer hydrate; b) the complete mono-layer hydrate; c) the bi-layer hydrate; d) the external hectorite surface.

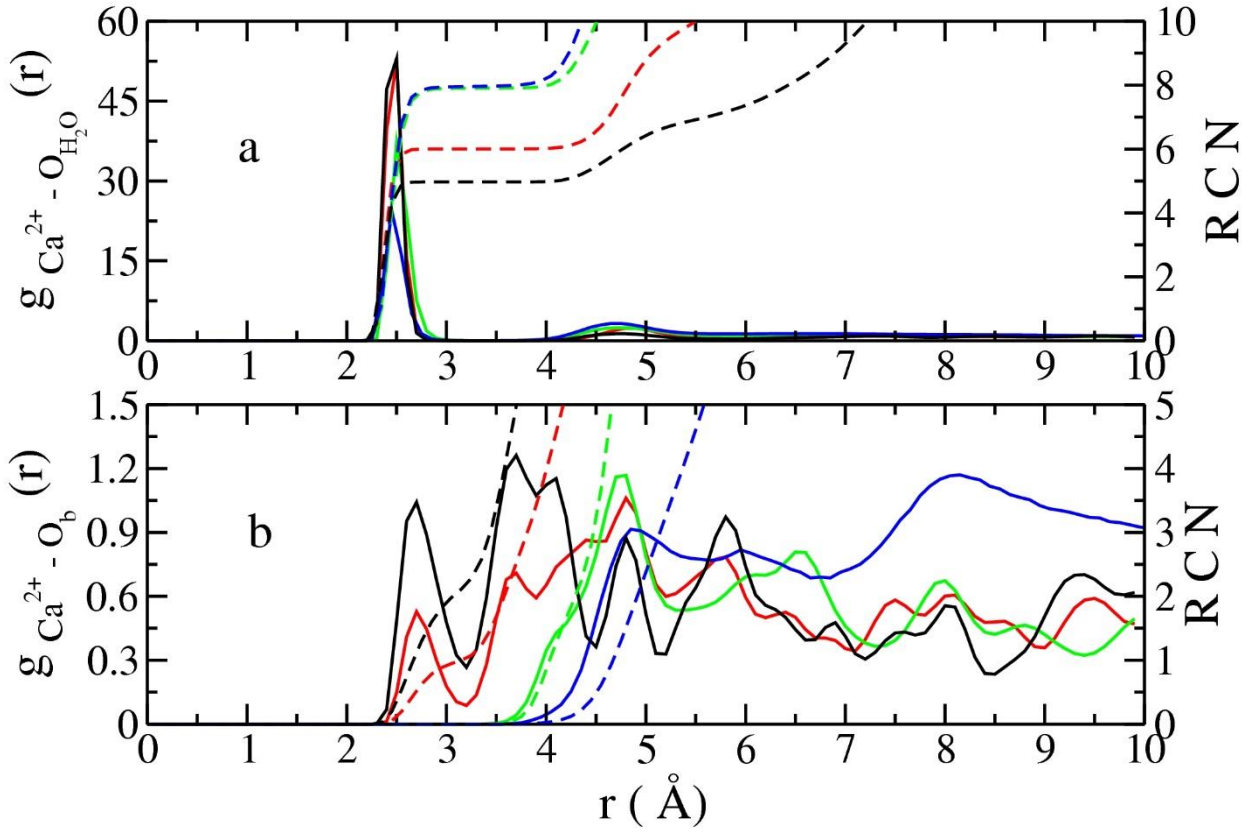

Figure 4. Radial distribution functions (solid lines) and the corresponding running coordination numbers (dashed lines) for atomic pairs in the interlayers and on the external surface of Ca-hectorites: a) Ca^{2+}-O_{H2O}; b) Ca^{2+}-O_b. Black – partial mono-layer hydrate; red – complete mono-layer hydrate; green – bi-layer hydrate; blue – external (001) surface.

a)

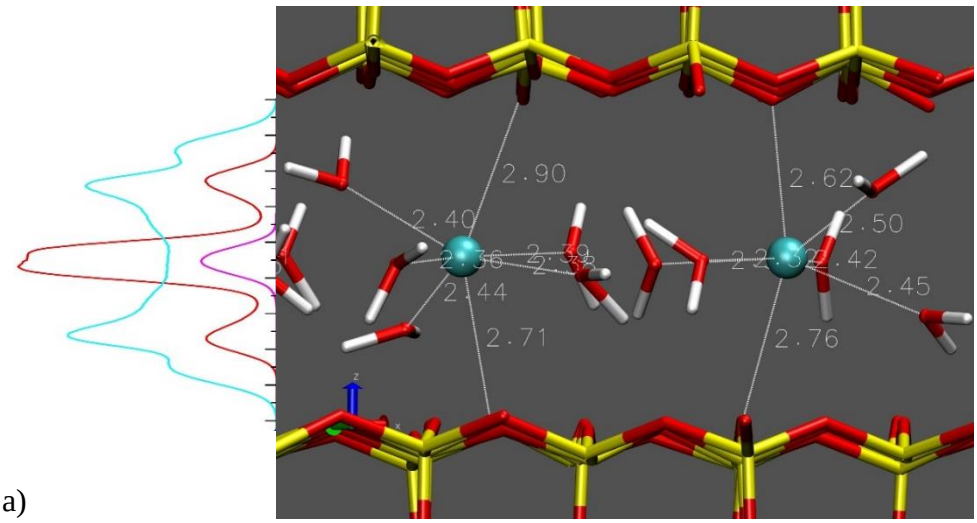

b)

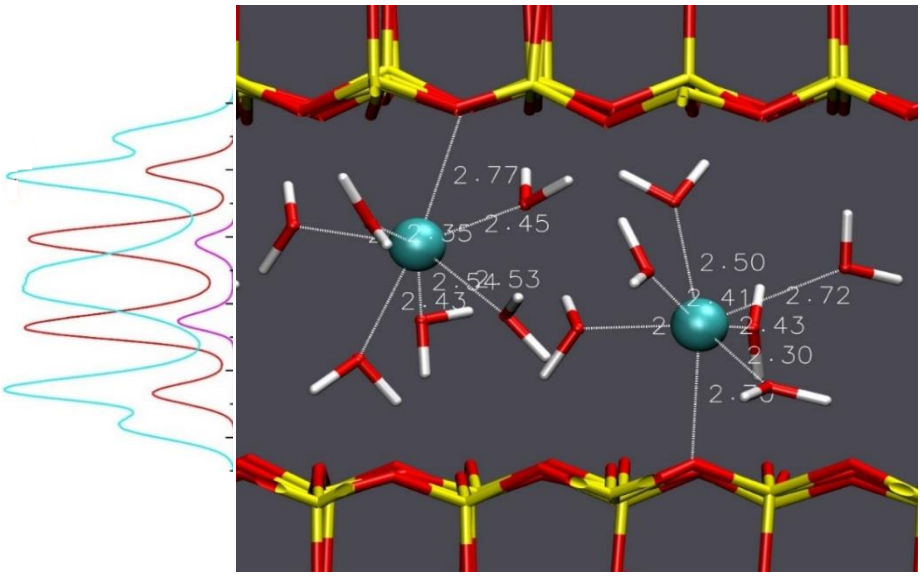

c)

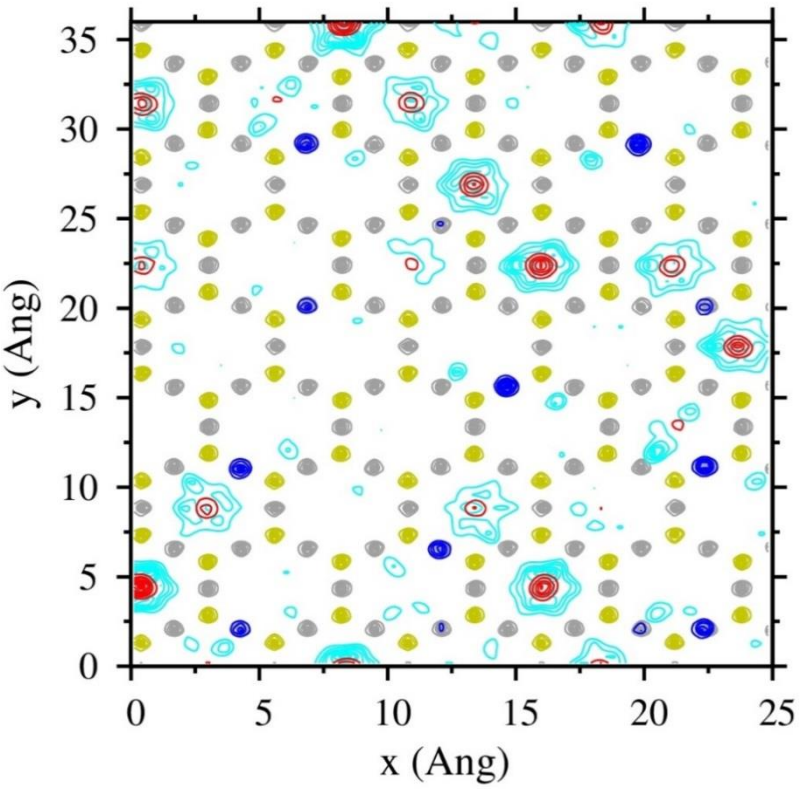

d)

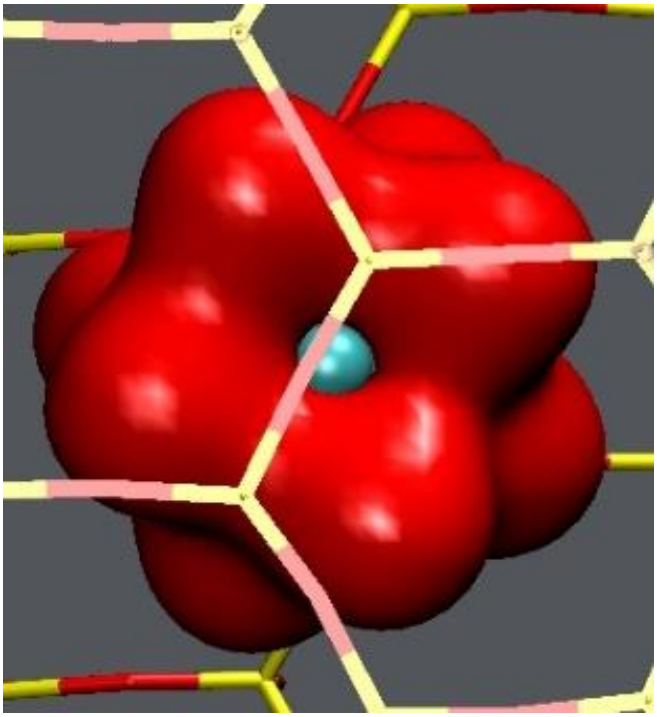

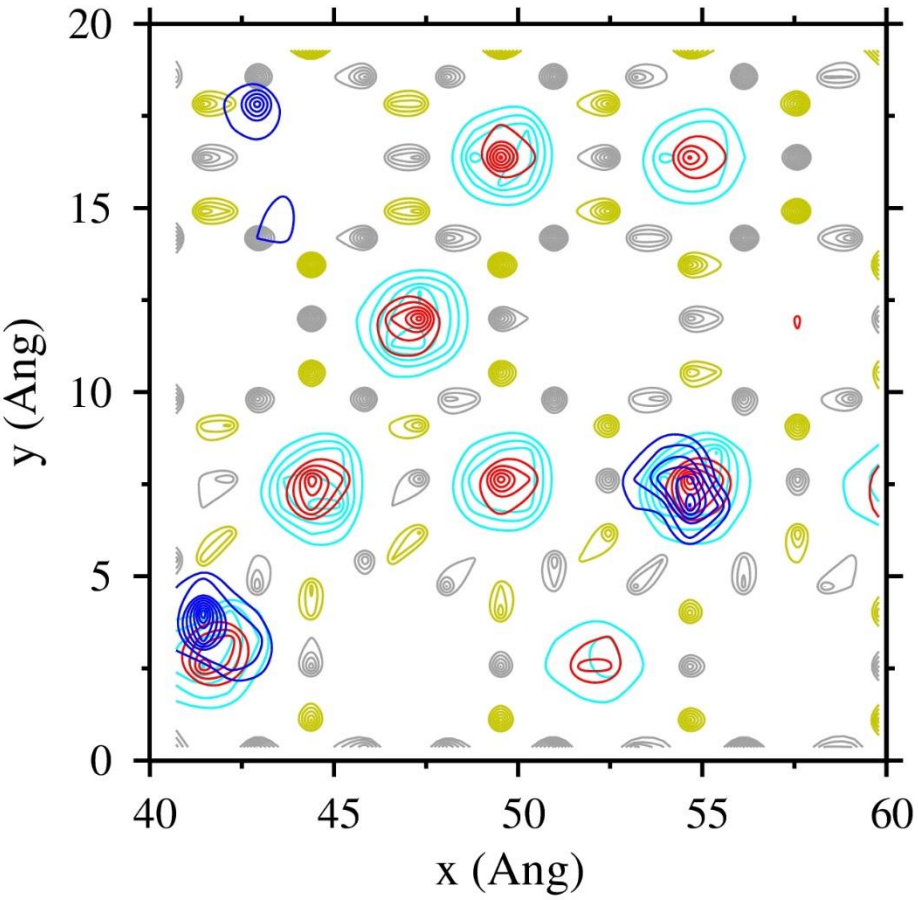

e)

Figure 5. Spatial arrangements of Ca^{2+} ions and H_2O molecules a) pictorial representation of the nearest H_2O molecules coordinating interlayer Ca^{2+} ions in partial monolayer hydrate; b) pictorial representation of the nearest H_2O molecules coordinating interlayer Ca^{2+} ions in complete monolayer hydrate; c) calculated PADDs of Ca^{2+} and H_2O molecules at $z < 2.2$ Å in bi-layer hydrate; d) pictorial representation of the near surface H_2O molecules coordinating an interlayer Ca^{2+} ion in bi-layer hydrate e) calculated PADDs of Ca^{2+} and H_2O molecules at $z < 2.2$ Å on external basal surface. Color code: O_b – gray, Si – yellow, Ca^{2+} – blue, O_{H2O} – red, H_{H2O} – cyan.

TOC Graphics